J Mater Sci (2006) 41:8244–8256
DOI 10.1007/s10853-006-1003-x

Computational analysis of the thermal conductivity of the carbon–carbon composite materials

M. Grujicic · C. L. Zhao · E. C. Dusel · D. R. Morgan · R. S. Miller · D. E. Beasley

Received: 5 August 2004 / Accepted: 14 October 2005 / Published online: 7 November 2006

Abstract Experimental data for carbon–carbon constituent materials are combined with a three-dimensional stationary heat-transfer finite element analysis to compute the average transverse and longitudinal thermal conductivities in carbon–carbon composites. Particular attention is given in elucidating the roles of various micro-structural defects such as de-bonded fiber/matrix interfaces, cracks and voids on thermal conductivity in these materials. In addition, the effect of the fiber precursor material is explored by analyzing PAN-based and pitch-based carbon fibers, both in the same type pitch-based carbon matrix. The finite element analysis is carried out at two distinct length scales: (a) a micro scale comparable with the diameter of carbon fibers and (b) a macro scale comparable with the thickness of carbon–carbon composite structures used in the thermal protection systems for space vehicles. The results obtain at room temperature are quite consistent with their experimental counterparts. At high temperatures, the model predicts that the contributions of gas-phase conduction and radiation within the micro-structural defects can significantly increase the transverse thermal conductivity of the carbon–carbon composites.

M. Grujicic (✉) · C. L. Zhao · E. C. Dusel ·
R. S. Miller · D. E. Beasley
Program in Materials Science and Engineering, Department of Mechanical Engineering, Clemson University,
241 Engineering Innovation Building, Clemson,
SC 29634-0921, USA
e-mail: mica.grujicic@ces.clemson.edu

D. R. Morgan
Touchstone Research Laboratory, Inc., Triadelphia,
WV 26059, USA

Nomenclature

α	Thermal accommodation factor
C_p	Solid-phase mass heat capacity
d	Gas collision diameter
δ	Characteristic length scale for gas molecules in the porous medium
ε	Emissivity
K_B	Boltzmann's constant
Kn	Knudsen number
k	Thermal conductivity
λ	Gas molecular mean field path
P	Pressure
Pr	Prandtle number
q	Heat flux
ρ	Density
σ	Stefan–Boltzmann constant
T	Temperature
x, y, z	Spatial coordinates

Subscripts

x–y	Quantity in the transverse plane
high	Graphene in-plane quantity
low	Graphene out-of-plane quantity

Superscripts

matrix	Matrix-phase quantity
fiber	Fiber-phase quantity
gas	Gas-phase quantity
r	Radiation related quantity

Introduction

Carbon–carbon composites comprise a family of materials, which have a carbon matrix and are reinforced with carbon fibers. A large variety of both fibers and matrix precursor materials and thermal processing schemes is used during fabrication of these materials. The choice of precursor materials and the thermal processing method used to fabricate the composites are the major factors which determine the thermo-physical properties of these materials [1]. Carbon–carbon composites are lightweight, high-strength material capable of withstanding temperatures over 3300 K in many environments. In these materials, high-strength, high-modulus carbon fibers are used to reinforce a carbon matrix in order to help resist the rigors of extreme environments.

Using special weaving techniques for the fibers, composite structures can be tailored to meet varied physical and thermal requirements. Woven reinforcements are either chemically vapor infiltrated or impregnated with resin or pitch and carbonized to yield finished, fully dense composites. Aerospace components such as rocket motor nozzle throats and exit cones, nose-caps/leading edges and thermal protection systems, in which reliable performance is the most critical requirement, are commonly fabricated from these materials. Advanced thermal protection systems envisioned for use on future hypersonic and space vehicles will likely be subjected to temperatures in excess of 2300 K and, therefore, will require the rapid conduction of heat away from the stagnation regions of wing leading edges, the nose cap area, and from engine inlet and exhaust areas. Since, carbon–carbon composite materials are lightweight, are able to retain their strength at high temperatures, and have high and tailorable thermal conductivity, they appear as very attractive candidates for the advanced thermal protection system applications [2].

In addition to the ability to withstand very high temperatures, future space vehicles will require carbon–carbon protective shields that can survive a temperature change from ca. 200 K to 2300 K (and an accompanying change in the environment) in a matter of minutes. Unfortunately, the experimental equipment which could simulate this variation is extremely expensive. Therefore, computer-based numerical models which can predict the thermo-mechanical response of these composite heat shields have become an invaluable tool for the determination of the necessary composite thickness, fiber architecture, and composite shape which yield optimal performance of the thermal protection system.

In a recent study, Klett et al. [3] carried out a two-dimensional computational analysis of thermal conductivity of the carbon–carbon composites at room temperature. Their analysis was applied separately to the planes orthogonal to and parallel with the carbon fibers, which enabled computation of the thermal conductivity in the direction collinear with the fiber axis.

The analysis was used to assess the effect of precursor material and thermal processing scheme for the carbon fibers and the carbon matrix, as well as the presence of micro-structural defects (primarily voids and cracks) on thermal conductivity of the carbon–carbon composites. Considering its two-dimensional and oversimplified character, the model proposed by Klett et al. [3] was reasonably successful in predicting the average thermal conductivity of standard pitch-based carbon–carbon composites at room temperature. The objective of the present work is to extend the computational analysis of thermal conductivity in the carbon–carbon composites carried out by Klett et al. [3] in order to: (a) include three-dimensional effects of the morphology and micro-structure of these materials; (b) incorporate the effects of gas-phase conduction and radiation within the micro-structural defects (e.g., de-bonded fiber/matrix interfaces, cracks and voids), and (c) to analyze the performance of these materials in space vehicle nose-cap and wings leading-edge applications.

The organization of the paper is as follows. In ''Thermal conductivities of the carban–carban composite constituents'' section, a brief overview is given of thermal conductivity of the two constituents in carbon–carbon composites, a carbon matrix and carbon fibers. In ''Thermal conductivities of the carban–carban composite constituents'' and ''Thermal conductivity of the gas phase'' sections, contributions of the gas-phase conduction and radiation within micro-structural defects to the heat transport are discussed, respectively. The definition of the boundary-value problem used to determine the transverse and the longitudinal components of thermal conductivity in the carbon–carbon composites is presented in section ''Governing equations—initial and boundary conditions''. The solution method used is discussed in section ''Computational method''. The results obtained in the present work are presented and discussed in ''Results and discussion''. The main conclusion resulted from the present work are summarized in ''Conclusions'' section.

Computational procedure

Thermal conductivities of the carbon–carbon composite constituents

As mentioned earlier, the two main constituent phases in a carbon–carbon composite are a carbon-based matrix and carbon-based fibers. In addition, carbon–carbon composites can generally contain a significant amount of cracks, voids and de-bonded fiber/matrix interfaces, which can yield a porosity level as high as 20%. In this section, a brief analysis is given of thermal conductivity of the two constituent phases since these represent the key input to the present finite element model for thermal conductivity of the carbon–carbon composites.

Matrix phase

Thermal properties of the carbon–carbon composite matrix depend on the precursor material and the processing route employed. In general, when the matrix phase is derived from a polymer, it is essentially structureless and, hence, its thermal conductivity is isotropic, i.e., $k_{xx} = k_{yy} = k_{zz}$, and $k_{xy} = k_{xz} = k_{yz} = 0$; where k is used to denote thermal conductivity, and x, y and z specify the components of the thermal conductivity matrix with respect to the three global Cartesian coordinates. When the carbon–carbon composite matrix is derived from a pitch, the matrix has the so-called "*sheath-like*" microstructure, within which carbon atoms are arranged in graphite crystallites, which tend to align themselves with the surface of the nearby fibers, Fig. 1(a). Since thermal conductivity is about two orders of magnitude higher within the (hexagonal) graphene planes relative to that in a direction normal to the graphene planes, thermal conductivity of a pitch-derived matrix is relatively high in the circumferential and longitudinal directions and relatively low in the radial direction, where these directions are defined relative to the center and the axis of the nearest carbon fiber. Hence, relative to a global Cartesian coordinate system in which the z-direction is aligned with the length of the nearest fiber, the thermal conductivity matrix for the carbon–carbon matrix phase can be defined as:

$$k_{\text{matrix}} = \begin{bmatrix} k_{\text{matrix}}^{\text{low}}\cos^2\theta + k_{\text{matrix}}^{\text{high}}\sin^2\theta & \left(k_{\text{matrix}}^{\text{low}} - k_{\text{matrix}}^{\text{high}}\right)\sin\theta\cos\theta & 0 \\ \left(k_{\text{matrix}}^{\text{low}} - k_{\text{matrix}}^{\text{high}}\right)\sin\theta\cos\theta & k_{\text{matrix}}^{\text{high}}\cos^2\theta + k_{\text{matrix}}^{\text{low}}\sin^2\theta & 0 \\ 0 & 0 & k_{\text{matrix}}^{\text{high}} \end{bmatrix} \quad (1)$$

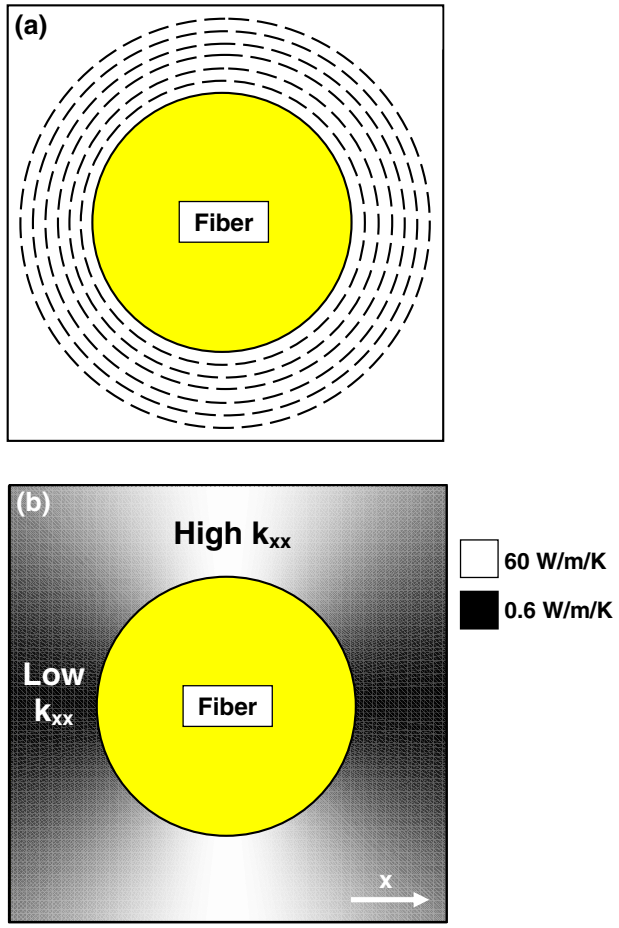

Fig. 1 (**a**) A schematic of the microstructure and (**b**) a field plot the *xx*-component of thermal conductivity for a pitch-based "sheath like" carbon matrix

where $k_{\text{matrix}}^{\text{high}}$ and $k_{\text{matrix}}^{\text{low}}$ are used to denote, respectively, the graphene in-plane and out-of-plane thermal conductivities of a pitch derived matrix and θ is an angle between the local radial direction and the x-axis.

A field plot for the xx component of the thermal conductivity matrix for a carbon–carbon matrix phase at typical values $k_{\text{matrix}}^{\text{high}} = 60$ W/m/K and $k_{\text{matrix}}^{\text{low}} = 0.6$ W/m/K is displayed in Fig. 1(b).

Fiber phase

Thermal conductivity of the fiber phase in carbon–carbon composites is also dependent on the precursor and the processing route used. In general, graphite crystallites in both the PAN-based and in pitch-based fibers give rise to a high thermal conductivity in the fiber-axis (longitudinal) direction. However, the transverse thermal properties in the two types of fibers are radically different. In the PAN-based fibers, the

normals of the graphite sheet-like crystallites are randomly oriented relative to global x (or y) axis. Consequently, the transverse thermal properties in these types of fibers are isotropic and the thermal conductivity matrix can be written as:

$$k_{\text{fiber}}^{\text{PAN}} = \begin{bmatrix} k_{\text{fiber}}^{x-y} & 0 & 0 \\ 0 & k_{\text{fiber}}^{x-y} & 0 \\ 0 & 0 & k_{\text{fiber}}^{z} \end{bmatrix} \tag{2}$$

where $k_{\text{fiber}}^{x\text{-}y}$ and k_{fiber}^{z} are used to denote the x–y in-plane (transverse) and the longitudinal thermal conductivity components of the PAN-derived fiber, respectively.

While pitch-based fibers generally exhibit the so-called "*flat-layer*" arrangement of their graphene crystallites, their transverse thermal conductivity is generally assumed to be radially symmetric (Fig. 2(a)) because of the random orientation of the flat-layer structure in different fibers and the fact that the fibers may be somewhat twisted around their axis. Under the radial symmetry assumption used, the graphite crystallites are assumed to fan out from the fiber center giving rise to a high-value of thermal conductivity in the radial direction and a low value of thermal conductivity in the transverse direction. The thermal conductivity matrix of the pitch-based fibers can then be defined as:

$$k_{\text{fiber}}^{\text{PAN}} = \begin{bmatrix} k_{\text{fiber}}^{\text{high}}\cos^2\theta + k_{\text{fiber}}^{\text{low}}\sin^2\theta & \left(k_{\text{fiber}}^{\text{high}} - k_{\text{fiber}}^{\text{low}}\right)\sin\theta\cos\theta & 0 \\ \left(k_{\text{fiber}}^{\text{high}} - k_{\text{fiber}}^{\text{low}}\right)\sin\theta\cos\theta & k_{\text{fiber}}^{\text{low}}\cos^2\theta + k_{\text{fiber}}^{\text{high}}\sin^2\theta & 0 \\ 0 & 0 & k_{\text{fiber}}^{z} \end{bmatrix} \tag{3}$$

where $k_{\text{matrix}}^{\text{high}}$ and $k_{\text{matrix}}^{\text{low}}$ are used to denote graphene in-plane and out-of-plane thermal conductivities of the fiber phase, respectively.

A field plot for the xx component of the thermal conductivity of the pitch-based fibers for typical values of $k_{\text{matrix}}^{\text{high}}$ = 110 W/m/K and $k_{\text{matrix}}^{\text{low}}$ = 1.1 W/m/K is displayed in Fig. 2(a).

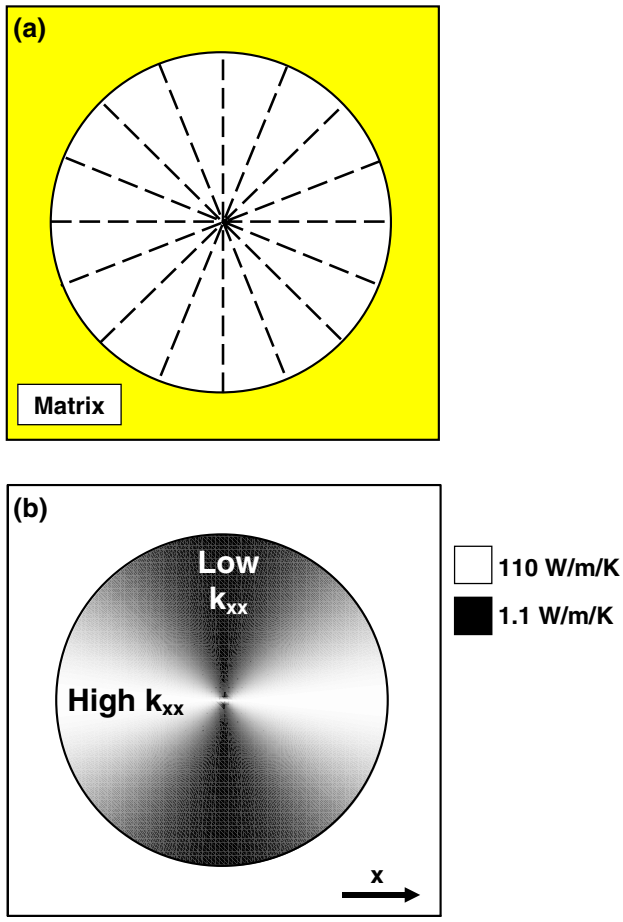

Fig. 2 (**a**) A schematic of the microstructure and (**b**) a field plot of the xx-component of thermal conductivity for a pitch-based carbon fiber

Thermal conductivity of the gas phase

As mentioned earlier, carbon–carbon composites typically contain micro-structural defects such as de-bonded fiber/matrix interfaces, cracks and voids. Hence, to correctly model thermal conductivity of the carbon–carbon composites, the heat transfer through de-bonded interfaces, voids and cracks must be considered. The heat transfer through such defects is generally considered to be dominated by gas-phase conduction and, at high temperatures, by radiation. Convective heat transfer is generally neglected due to the fact that the gas phase is confined to very small volumes of the defects and, hence, a long-range motion of the gas phase is prevented. In the present section, a brief analysis is given of the heat transfer by gas-phase conduction.

While thermal conductivity of the solid materials generally shows weak temperature and pressure dependences, thermal conductivity of the gas is typically a very sensitive function of both temperature and pressure. Following Sullins and Daryabeigi and co-workers [4], thermal conductivity of the gas phase can be defined as:

$$k_{\text{gas}} = \frac{k_{\text{gas,o}}}{\Phi + \Psi \cdot 2\frac{2-\alpha}{\alpha}\frac{2\cdot\gamma}{\gamma+1}\frac{1}{Pr}Kn} \tag{4}$$

where k_{gas},o is temperature-dependent thermal conductivity of the gas phase at the atmospheric pressure,

α is a thermal accommodation factor (a fraction of gas molecules which come into thermal equilibrium with the solid phase during collision with the surface of the solid phase), γ is a constant-pressure over constant-volume specific heats ratio, *Pr* is the Prandtle number, and *Kn* is the Knudsen number. Parameters Φ and Ψ depend on the gas-phase regime, i.e., on the magnitude of the Knudsen number: For $Kn \leq 0.01$ (i.e., for the continuum gas-phase regime), $\Phi = 1$ and $\Psi = 0$, and thus $k_{gas} = k_{gas,o}$; for$0.01 \leq Kn \leq 10$ (i.e., for the transition regime), $\Phi = 1$ and $\Psi = 1$; and for $Kn \geq 10$ (i.e., for the free-molecules gas-phase regime), $\Phi = 0$ and $\Psi = 1$.

The Knudsen number is defined as:

$$Kn = \frac{\lambda}{\delta} \tag{5}$$

where the gas molecular mean field path, λ, is defined as:

$$\lambda = \frac{K_B T}{\sqrt{2}\pi P d_g^2} \tag{6}$$

and δ, the characteristic length scale for gas molecules within the micro-structural defects.

A list of thermo-physical parameters for the gas (nitrogen) used in the present work is given in Table 1.

Radiative thermal conductivity

At relatively high temperature, the radiative heat transfer within micro-structural defects of the carbon–carbon composites may become significant and, hence, must be considered when modeling thermal conductivity of these materials. In our recent work [5], a detailed analysis of the radiative heat transfer was analyzed within a carbon-foam material by solving the radiative heat transfer equation for a plane-parallel, isotropically scattering, homogeneous, gray (i.e., frequency invariant) medium with azimuthal symmetry. The results of this analysis established two important facts: (a) the role of radiation in heat transfer within the pores can be reasonably well accounted for by adding its contribution to thermal conductivity, and by subsequently considering only the conductive heat transfer but with a radiation-modified (effective) thermal conductivity; (b) A simple model, presented below, can be used with a reasonable success over a wide temperature range to quantify the contribution of radiation to the effective thermal conductivity.

The steady-state radiative heat flux, q_r, between two parallel planes (i.e., two opposing faces of a defect) can be defined as:

$$q_r = \varepsilon\sigma\left(T_2^4 - T_1^4\right) \tag{7}$$

where ε is the surface emissivity, σ is the Stefan–Boltzmann constant, and T_1 and T_2 are the temperatures of the two planes.

Assuming that $T_2 \cong T_1$, Eq. (7) can be rewritten as:

$$q_r = -4\varepsilon\sigma T^3\delta\frac{}{\delta} \approx -4\varepsilon\sigma T^3\delta\frac{dT}{dx} \tag{8}$$

where $T \equiv 0.5(T_1 + T_2)$ and $\Delta T \equiv T_1 - T_2$.

From the second Eq. (8), it is clear that the contribution of radiation to thermal conductivity can be defined as:

$$k_{rad} = 4\varepsilon\sigma\delta T^3\delta \tag{9}$$

Since gas-phase conduction and radiation within the micro-structural defects take place in parallel, the effective thermal conductivity of the medium residing within such defects is defined as a sum of k_{gas} and k_{rad}.

Governing equations—initial and boundary conditions

As stated in the previous section, the role of radiation in the heat transfer through the micro-structural defects can be accounted for by defining an effective thermal conductivity which incorporates both the

Table 1 Thermo-physical properties for nitrogen gas used in the present work

Property	Symbol	Unit	Value	Equation where first used
Collision diameter for nitrogen gas	d_g	m	3.74×10^{-10}	Eq. (6)
Specific heat ratio for nitrogen gas	γ	N/A	1.4	Eq. (4)
Thermal accommodation factor for nitrogen	α	N/A	1	Eq. (4)
1 tam pressure thermal conductivity of nitrogen gas	$k_{gas,o}$	W/m-K	$1.3 \times 10^{-11}T^3 - 4.5 \times 10^{-8}T^2 + 9.4 \times 10^{-5}T + 0.0014$	Eq. (4)
Prandtle number of nitrogen gas	*Pr*	N/A	$-2.1 \times 10^{-10}T^3 + 5.5 \times 10^{-7}T^2 - 0.00038T + 0.79$	Eq. (4)

effects of gas-phase conduction and radiation. Once such effective thermal conductivity is defined, the problem of the heat transfer through a carbon–carbon composite can be treated as a pure conduction problem. Consequently, the heat transfer problem in one of the Cartesian directions is governed by the following energy conservation equations:

$$\rho C_p \frac{\partial T}{\partial t} = \frac{\partial}{\partial v}\left(k \frac{\partial T}{\partial v}\right) = 0, (v = x, y, z) \tag{10}$$

where ρ is the material density, C_p is the mass heat capacity, k is the effective thermal conductivity, T is the temperature, t is the time, and x, y, z are the spatial coordinates.

To complete the definition of the steady-state heat conduction problem, the boundary conditions must be assigned to Eq. (10). To determine the xx (transverse) component of thermal conductivity, the following boundary conditions are employed:

$$T(x = 0) = T_o + \Delta T \tag{11}$$

$$T(x = a) = T_o \tag{12}$$

$$q_y(y = 0) = q_y(y = a) = 0 \tag{13}$$

$$q_z(z = 0) = q_z(z = a) = 0 \tag{14}$$

where T_o and ΔT are a constant temperature and a constant temperature difference, a is the edge-length a the cubic computational domain, and q_y and q_z denote the heat fluxes in the y- and z-direction. A schematic of the boundary value problem is given in Fig. 3.

The corresponding boundary conditions for determination of the yy (transverse) and zz (longitudinal) components of thermal conductivity can be readily defined by interchanging, x, y and z.

Computational method

The governing nonlinear differential equation, Eq. (10), subjected to the boundary conditions, Eqs. (11)–(14), is implemented in the commercial mathematical package FEMLAB [6] and solved for the dependent variable, the temperature, using the finite element method. FEMLAB provides a powerful interactive environment for modeling various scientific and engineering problems and for obtaining the solution for the associated (stationary and transient, both linear and nonlinear) systems of governing partial differential equations. FEMLAB is fully integrated with the MATLAB, a commercial mathematical and visualization package [7]. As a result,

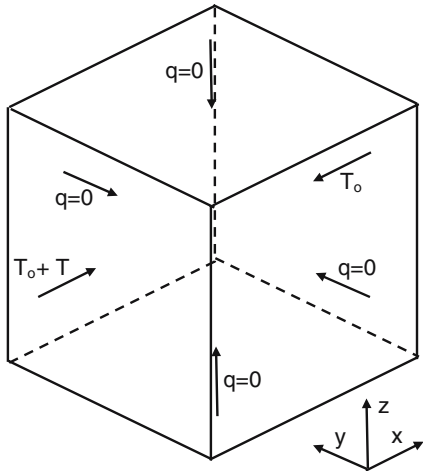

Fig. 3 A schematic of the boundary value problem used during finite element determination of thermal conductivity of carbon–carbon composites

the models developed in FEMLAB can be saved as MATLAB programs for parametric studies or iterative design optimization.

The governing differential equation, Eq. (10), and the boundary conditions, Eqs. (11)–(14), are implemented in FEMLAB using the so-called "*General Form*" for nonlinear partial differential equations. Within this approach, a boundary value problem (like the one at hand) is cast into the following form:

$$d_{ij}\dot{u}_j + \nabla \cdot \Gamma_i = F_i \quad \text{over the computational domain, and} \tag{15}$$

$$-n \cdot \Gamma_i = G_i + \frac{\partial R_m}{\partial u_i} v_m \quad \text{the Neumann boundary conditions and/or} \tag{16}$$

$$0 = R_m \quad \text{the Dirlichlet boundary conditions} \tag{17}$$

where j, j = 1, 2, ..., number of differential equations in the system, u are dependent variables, a raised dot is used to denote the time derivative, $\nabla\cdot$ is a divergence operator d_{ij} is a coefficient matrix, Γ, F, G and R are, in general, functions of the spatial coordinates, the dependent variable or space derivatives of the dependent variables and v is the Lagrange multiplier. Furthermore, Γ is a flux vector while F, G and R are scalars.

The boundary value problem defined by Eqs. (10)–(14) is then cast as follows to be consistent with FEMLAB general form.

The Governing Equation:

$$\begin{bmatrix} \frac{\partial}{\partial x} \\ \frac{\partial}{\partial y} \\ \frac{\partial}{\partial z} \end{bmatrix}^{\mathrm{T}} \begin{bmatrix} k_{xx} & k_{xy} & k_{xz} \\ k_{yx} & k_{yy} & k_{yz} \\ k_{zx} & k_{zy} & k_{zz} \end{bmatrix} \begin{bmatrix} \frac{\partial T}{\partial x} \\ \frac{\partial T}{\partial y} \\ \frac{\partial T}{\partial z} \end{bmatrix} = 0 \tag{18}$$

The Dirlichlet boundary condition at the boundaries normal to the direction of heat conduction:

$$0 = T - (T_{\mathrm{o}} + \Delta T) \quad \text{at } x = 0 \tag{19}$$

$$0 = T - T_{\mathrm{o}} \quad \text{at } x = a \tag{20}$$

The Neumann boundary conditions at the remaining boundaries:

$$\begin{bmatrix} n_1 \\ n_2 \\ n_3 \end{bmatrix}^{\mathrm{T}} \begin{bmatrix} k_{xx} & k_{xy} & k_{xz} \\ k_{yx} & k_{yy} & k_{yz} \\ k_{zx} & k_{zy} & k_{zz} \end{bmatrix} \begin{bmatrix} \frac{\partial T}{\partial x} \\ \frac{\partial T}{\partial y} \\ \frac{\partial T}{\partial z} \end{bmatrix} = 0 \tag{21}$$

where

$$\begin{aligned} &n_1 = 0, n_2 = -1, n_3 = 0, \quad \text{at } y = 0; \\ &n_1 = 0, n_2 = 1, n_3 = 0, \quad \text{at } y = a; \\ &n_1 = 0, n_2 = 0, n_3 = -1, \quad \text{at } z = 0 \quad \text{and;} \\ &n_1 = 0, n_2 = 0, n_3 = 1, \quad \text{at } z = a. \end{aligned}$$

Thermal conductivity of the carbon–carbon composites is analyzed at two different length scales: (a) At a ''micro'' scale which is comparable with the diameter of carbon fibers. A typical finite element mesh used in this type of analysis, containing four carbon fibers is shown in Fig. 4(a). Within this type of analysis, the only defects allowed were de-bonded fiber/matrix interfaces. To comply with the experimental results of Klett et al. [3], the diameter for all fibers is set to 14 μm, and the cubic-domain edge-length adjusted to yield the specified volume fraction of the fibers. At a given fraction of the de-bonded fiber/matrix interface, the micro-scale finite element analysis is carried out repeatedly for randomly placed de-bonded interfacial sections and the mean value and the standard deviation of thermal conductivity monitored as a function of the number of analyses carried out. After about 2000 analyses, the mean value and the standard deviation of thermal conductivity are found to converge to essentially constant values. At that point, all the values of thermal conductivity are used to construct a probability density plot for the microscopic thermal conductivity. (b) At the ''macro'' scale, the edge-length of the cubic computational cell is set comparable to the thickness of carbon–carbon thermal protection structures in the nose cap and leading edges of the space vehicles. A schematic of the typical finite element mesh used in this type of analysis is shown in Fig. 4(b). Within this type of analysis, a fraction of the cubic finite elements consistent with the volume fraction of voids and cracks is selected and assign the effective thermal properties governed by gas-phase conduction and radiation, as discussed in sections ''Thermal conductivity of the gas phase'' and ''Radiative thermal conductivity''. Thermal conductivity of the remaining cubic elements is assigned at random using the probability density generated via the micro-scale finite

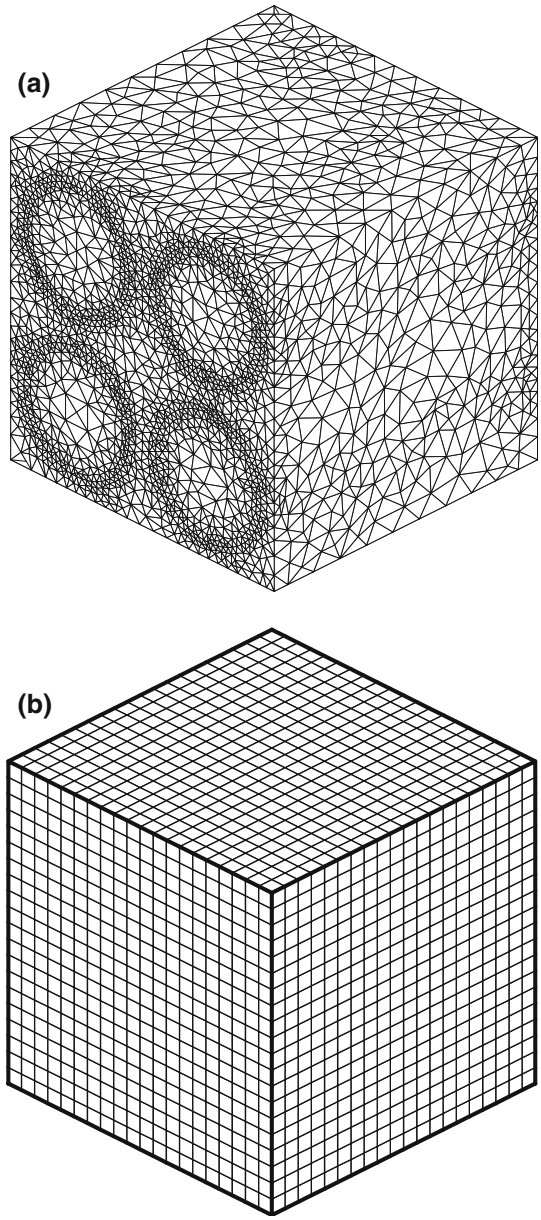

Fig. 4 Typical finite element meshes used during: (**a**) micro-scale and (**b**) macro-scale analysis of thermal conductivity of the carbon–carbon composites

element analysis discussed above. As in the case of micro-scale analysis, the calculations are repeated and the mean values of microscopic thermal conductivity and standard deviation monitored as a function of the number of simulations. The mean values and the standard deviations are found to converge to effectively constant values after about 1,600 calculations. In ''Results and discussion'' section, error bars are used to denote one standard-deviation variations for the macroscopic thermal conductivities.

It should be noted that the magnitude of the standard deviation of thermal conductivity, in addition to the magnitude of thermal conductivity itself, is a very important parameter in the selection of a high-temperature insulating structural material. Materials with smaller values of the standard deviation are generally preferred since they enable more robust designs. Unfortunately, in the present work, no statistical difference was found between the materials based on the PAN-based and the pitch-based fibers.

Standard mesh sensitivity and model robustness analyses were carried out following the procedure outlined in our recent work [8]. The results of these analyses validated that the model developed is mesh-insensitive and robust but the results will not be presented here for brevity.

Results and discussion

Effect of fiber type on the transverse heat flow

Following Klett et al. [3], carbon–carbon composites composed of a pitch-based AR-120 carbon matrix and either PAN-based T300 or pitch-based P55 carbon fibers are analyzed. As discussed in ''Thermal conductivities of the carban–carban composite constituents'' section, the matrix has a sheath-like structure, T300 fibers are thermally isotropic while P55 fibers have radially symmetric thermal properties. Thermal properties of these constituents of the carbon–carbon composites are listed in Table 2. To show qualitatively how the selection of the carbon fibers between T300 and P55, affects the flow of heat in the transverse (normal to the fiber axis) direction, vector plots for the heat flux for the two choices of carbon fibers are shown in Fig. 5(a) and (b), respectively. In Fig. 5(a) and (b), a small overall temperature gradient is applied in the (horizontal) x-direction, while zero-flux conditions are applied in the remaining two directions.

The results displayed in Fig. 5(a) and (b) clearly show that the heat in the matrix tend to propagate along the graphene planes. As far as the carbon fibers are concerned, in the case of thermally isotropic PAN-based T300 fibers (Fig. 5(a)), the heat flows uniformly in the$x$-direction through the carbon fibers. In the case of pitch-based P55 fibers (Fig. 5(b)), on the other hand, the heat clearly propagates along the radially oriented graphene planes.

Validation of the model at room temperature

The work of Klett et al. [3] provides a comprehensive set of experimental data for room-temperature thermal conductivity of AR-120 pitch-based carbon matrix/T300 PAN-based carbon fiber and AR-120 carbon matrix/P55 pitch-based carbon fiber based carbon–carbon composites. For the experimental data reported

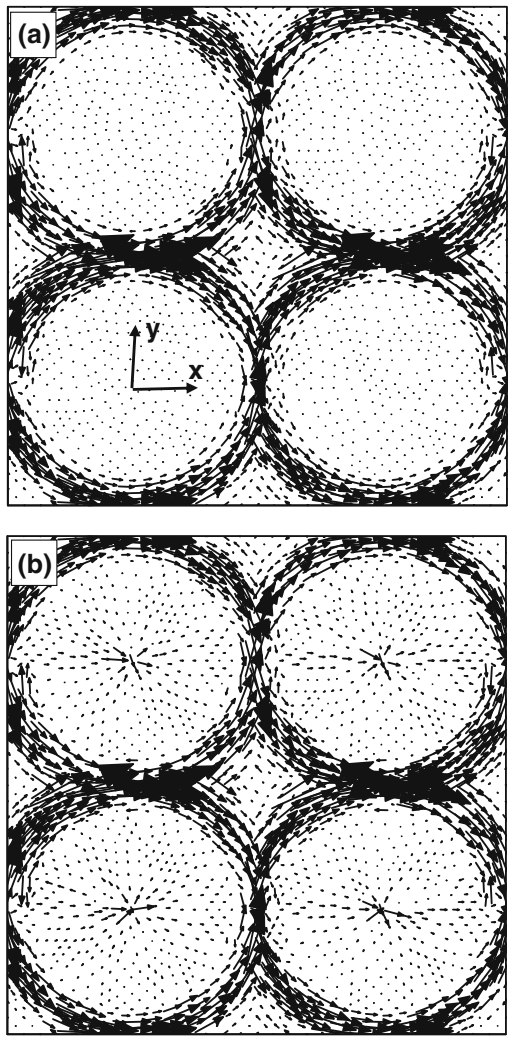

Fig. 5 Vector plots for the x-component of heat flux in a carbon–carbon composite with a pitch-based sheath-like carbon matrix and: (**a**) thermally isotropic PAN-based and (**b**) thermally radially symmetric pitch-based carbon fibers

by Klett et al. [3], the corresponding fiber volume fractions and porosity levels are specified. However, the extent of fiber/matrix interfacial de-bonding was not provided. Since such interfacial de-bonding can significantly affect transverse thermal conductivity of the carbon–carbon composites, the fraction of the interface de-bonded was assumed to vary between 0 and 0.5, while the width of interfacial gaps was varied between 0.1 and 1.0 μm. The corresponding results for the indicated range of the width of interfacial gaps are found to differ only 0.2–0.5%. Consequently, all the results reported here pertain to the width of interfacial gaps of 0.5 μm.

A comparison between the experimental room-temperature transverse and longitudinal thermal conductivities and their model counterparts at various levels of the fiber volume fraction and the porosity is given in Figs. 6 and 7, respectively. In Figs. 6 and 7, solid symbols are used to denote the experimental data while open symbols are used to denote model-predicted results. For the model results, solid lines are used to denote perfectly bonded fiber/matrix interfaces while dashed lines are used to denote the data pertaining to a 50% level of interfacial decohesion.

In general, the agreement between the experimental and computed thermal conductivities is reasonable at all levels of the fiber volume fraction and porosity. For the transverse thermal conductivity, Fig. 6, the agreement is generally better for the case of a 50% interfacial decohesion. This finding is consistent with Klett et al. [3] who reported that the carbon–carbon composites had a significant fraction of interfacial de-bonding. In the case of the longitudinal thermal conductivity, on the other hand, interfacial de-bonding seems to have a minimal effect. This is consistent with the fact that de-bonded fiber/matrix interfaces do not

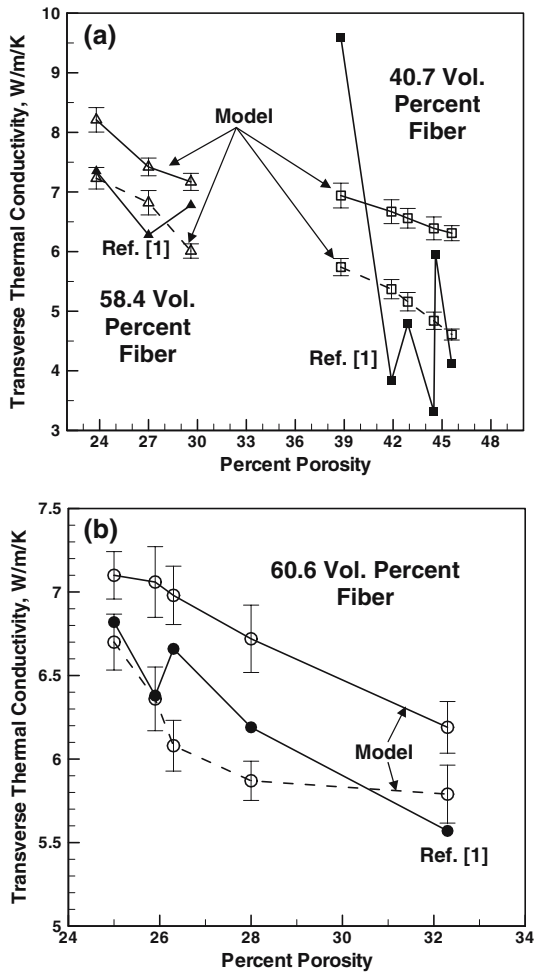

Fig. 6 A comparison between the measured and model predicted transverse thermal conductivity in AR-120 carbon matrix/T300 carbon fiber carbon–carbon composites heat treated at 2673 K

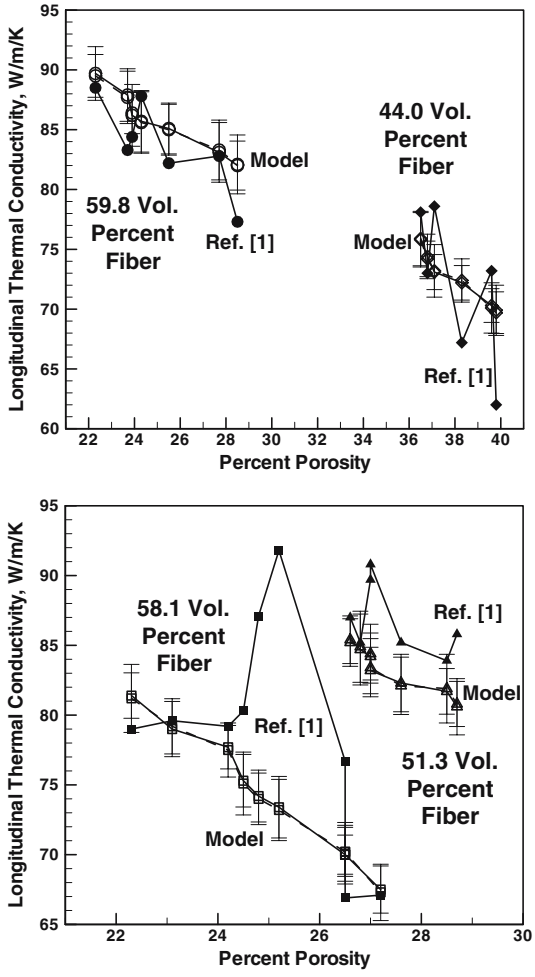

Fig. 7 A comparison between the measured and model predicted longitudinal thermal conductivity in AR-120 carbon matrix/T300 carbon fiber carbon–carbon composites heat treated at 2673 K

hamper heat flow in the direction parallel with the fibers axis and the fact that interfacial de-bonded regions occupy a small fraction of the material volume.

As expected, both the experimental and model results presented in Fig. 6 show that the room-temperature transverse thermal conductivity in pitch-based carbon-matrix/PAN-based carbon-fibers carbon–carbon composites is reduced by the presence of cracks- and voids-induced porosity. In addition, the model predicts that fiber/matrix interfacial decohesion can also significantly affect the transverse thermal conductivity of carbon–carbon composites. To get a more complete view of the effect of porosity on the transverse thermal conductivity of carbon–carbon composites with either PAN-based or pitch-based carbon fibers, the respective transverse thermal conductivity contour plots are given in Fig. 8(a) and (b).

The results displayed in Fig. 8(a) and (b) show that both cracks/voids and interfacial de-bonding lower the transverse thermal conductivity of carbon–carbon composites. However, the relative effects of cracks/voids and interfacial de-bonding are somewhat affected by the type (PAN-based vs. pitch-based) carbon fibers. In the case of thermally isotropic PAN-based fibers, cracks and voids seem to have a more pronounced effect than in the case of thermally radially symmetric pitch-based fiber. This finding is consistent with the fact that in the case of pitch-based fiber, heat transfer along the high-conductivity radial directions is significant (Fig. 5(b)), and interfacial de-bonding hampers the heat transfer between the fibers and the matrix. On the other hand, since the heat transfer in a direction normal to the fiber axis is significantly smaller in the case of PAN-based fibers even for the perfectly bonded fiber/matrix interfaces (Fig. 5(a)), interfacial de-bonding is not expected to affect the transverse thermal conductivity significantly.

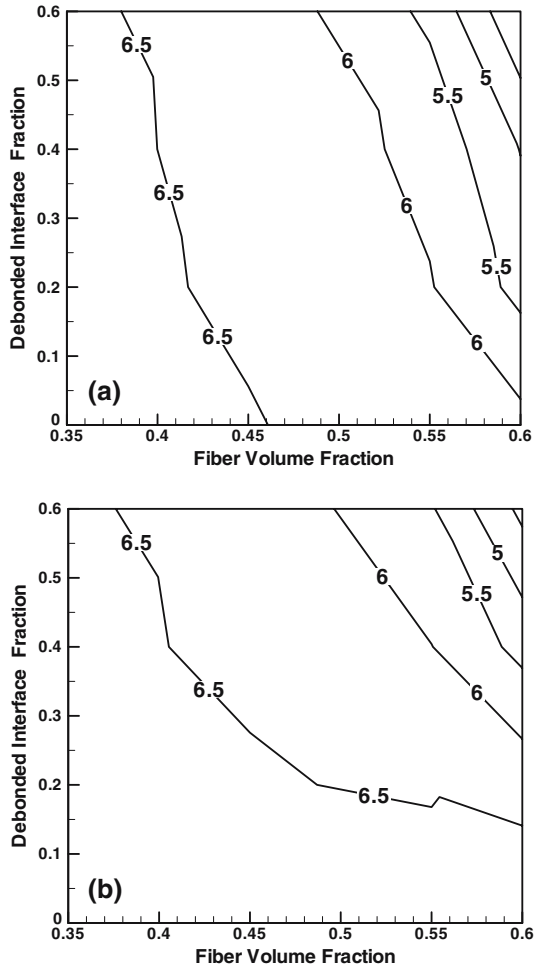

Fig. 8 Typical variations of the transverse thermal conductivity in carbon–carbon composites containing: (**a**) PAN-based and (**b**) pitch-based carbon fibers with porosity and fiber/matrix interfacial de-bonding

The role of gas conduction and radiation in heat transfer

Up to this point, the focus of this paper has been the analysis of thermal conductivity in carbon–carbon composites at room temperature and 1 atm pressure. The effect of temperature and pressure on the gas-phase conductivity and radiative thermal conductivity in cracks/voids (δ = 14 μm) and de-bonded interfacial gaps (δ = 0.5 μm) is shown in Fig. 9(a) and (b), respectively. The results shown in Fig. 9(a) and (b), in connection with the thermal conductivity data listed in Table 2, suggest that the contribution of heat transfer through the micro-structural defects is negligible at room temperature. However, the results and the data do imply that at elevated temperatures, such as those experienced by a space shuttle's nose cap and leading wing edges during re-entry, the contribution of gas-phase conduction and radiation may be significant.

The main concern in utilizing carbon–carbon composites for thermal protection systems is the potential increase in transverse thermal conductivity. In carbon–carbon composite thermal protection systems, the carbon fibers are aligned with the surface of the structure they are protecting. This alignment allows for the heat to be conducted away from the places (e.g., nose cap and leading edges) subjected to the highest temperatures and redirected to the outer sections of the vehicle much less likely to experience the effects of aerodynamic heating. At the same time, a relatively small amount of heat would be transferred through the thickness of the carbon–carbon structure.

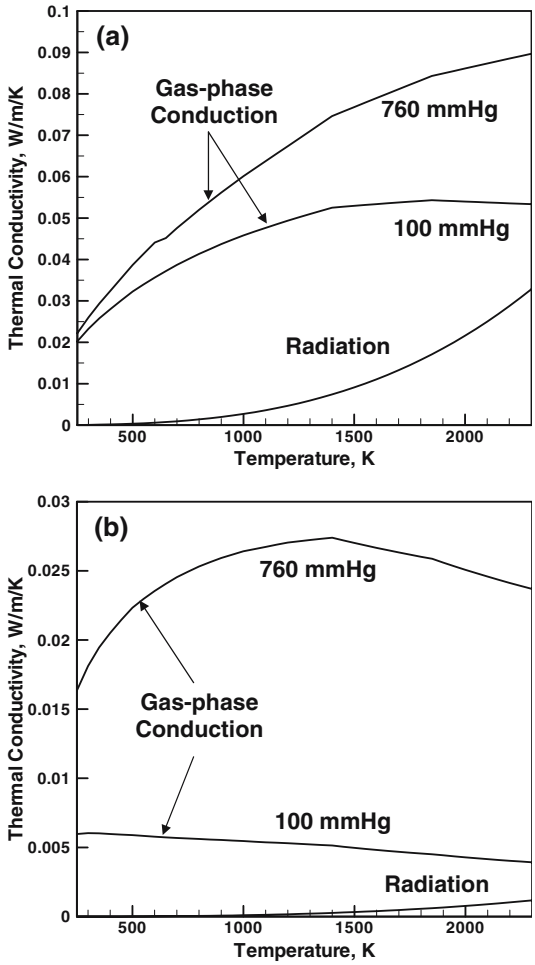

Fig. 9 Effect of temperature and pressure on the gas-phase and radiative thermal conductivities within: (**a**) typical cracks/voids and (**b**) de-bonded interfacial gaps

To assess the potential effect of gas-phase conduction and radiation on the through-the-thickness heat transfer in carbon–carbon thermal protection shields, the boundary value problem defined in ''''Governing equations—initial and boundary conditions'' section is redefined and solved using the same method presented in ''Computational method'' section.

The governing equation, Eq. (10), is utilized once more but this time in the transient state. In other words, the rightmost side of this equation is not set to zero. The first boundary condition defined in Eq. (11) is replaced with a condition, $T(x = 0,\ t) = T_{\text{out}}(t)$, where $T_{\text{out}}(t)$ is the time dependant temperature variation of the outer surface of the thermal protection structure. A typical T_{out} vs. t profile taken from [9] is reproduced in Fig. 10(a). The second boundary condition is redefined as $q_x\ (x = a, t) = 0$, and corresponds to an adiabatic condition at the inner surface of the thermal protection structure. The remaining boundary conditions, Eqs. (12)–(14) are kept unchanged.

The variation of environmental pressure with time during vehicle re-entry also taken from [9] is given in Fig. 10(b). This variation is needed during computation of the gas-phase conductivity. It should be noted that by allowing the pressure within micro-structural defects to be equal to the ambient pressure, one assumes that these defects are interconnected and propagate to the surface of the structure which may not be fully realistic.

The results of this calculation yielded a variation of temperature at the inner surface of a 6.35 mm-thick carbon–carbon thermal protection structure. The inclusion of gas-phase conduction and radiation through the micro-structural defects under the assumption of a temperature-invariant solid-phase thermal conductivity is found to give rise to an 18–21 K increase in the maximum temperature of the inner surface of the structure. This temperature increase is significant considering the fact that the maximum allowable temperature of the inner surface is generally set to 450 K to ensure structural integrity of the aluminum structure of the vehicle and that in order to compensate for a 20 K temperature increase, the thermal insulation thickness may need to be increased by about 1 cm [9].

As stated earlier, in the aforementioned analysis the thermal conductivity of the carbon matrix and the carbon fibers was assumed not to change with temperature. This was done because the variation of

Table 2 Components of thermal conductivity of the carbon–carbon constituent materials

Material/heat treating temperature	Component of thermal conductivity, W/m-K		
	Radial	Circumferential	Longitudinal
T300-Fiber/PAN 1373 K	0.085	0.085	8.5
T300-Fiber/PAN 2673 K	0.76	0.76	76
P55-Fiber/Pitch 1373 K	113	1.13	113
P55-Fiber/Pitch 2673 K	196	1.96	196
Pitch-Matrix 1373 K	0.06	6.2	6.2
Pitch-Matrix 2673 K	0.64	64.3	257

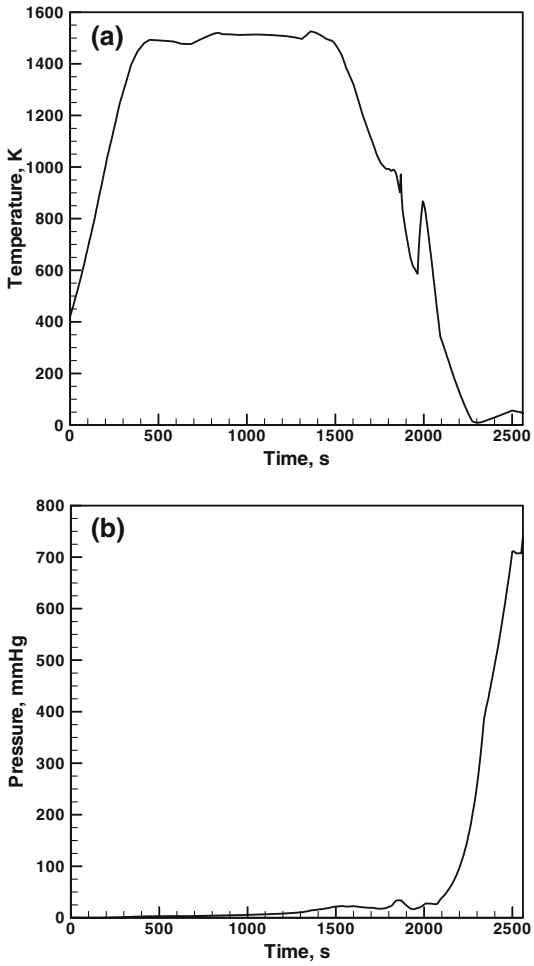

Fig. 10 Typical: (**a**) radiation equilibrium temperature and (**b**) pressure profiles associated with a specific location of the thermal protection system of a space vehicle during re-entry

thermal conductivity with temperature for the matrix and the fibers were not available. To overcome this limitation, it is assumed that the temperature dependence of the thermal conductivity of the materials at hand was comparable and, hence, can be approximated with the temperature-dependent thermal conductivity in the grade of POCO graphite with the identical room-temperature thermal conductivity [10]. Typically, POCO graphites have their thermal conductivity decrease by between 35% and 60%, as the temperature is increased from the room temperature to approximately 1,900 K with the larger decrease observed in the graphite grades with a high room-temperature thermal conductivity. The incorporation of the temperature-dependent thermal conductivities for the matrix and the fiber materials in the present transient thermal analysis yielded three important results:

(a) The inner temperature decreased by between 26° and 31° relative to the case when the solid-phase thermal conductivity is assumed to be constant;
(b) The micro-structural defects give rise to a practically identical increase in the temperature of the inner surface for the case of temperature-dependent solid-phase conductivity as for the temperature-independent solid-phase conductivity; and
(c) The effect of micro-structural defects on high-temperature thermal conduction is found to be lass pronounced in the case of the material containing PAN-based fibers relative to that in the material based on pitch-based fibers. This finding can have an important effect on the selection of the type of the carbon–carbon composite in high-temperature applications in which the material can continue to develop micro-structural defects while in service. Under such conditions, the materials whose properties (thermal conductivity in the present case) is less microstructure sensitive is typically the preferred choice.

Conclusions

Based on the results obtained in the present work, the following main conclusions can be drawn:

1. Carbon-matrix and carbon-fiber precursor materials and processing treatment affect both the heat-flow fields and the effective thermal conductivity of the carbon–carbon composites. In general, the heat-flow fields and thermal conductivity are dominated by the local orientation of the graphene planes which have a high in-plane thermal conductivity.
2. Micro-structural defects such as cracks, voids, and de-bonded fiber/matrix interfaces can significantly lower the thermal conductivity, in particular, the transverse thermal conductivity. While such defects can somewhat compromise the mechanical integrity of the thermal protection structures, their role in reducing through-the-thickness heat flow is quite beneficial.
3. While at near-room temperatures, heat transfer through the micro-structural defects is highly limited. On the other hand, the gas-phase conduction and radiation within such defects can make significant contributions to the overall thermal conductivity of carbon–carbon composites at high temperatures and near-atmospheric and super-atmospheric pressures.

Acknowledgements The material presented in this paper is based on work sponsored by the U.S. Air Force through Touchstone Research Laboratory, Ltd. The authors acknowledge valuable discussions with Professors Don Beasley, Richard Miller and Jay Ochterbeck of Clemson University.

References

1. Buckley JD, Edie DD (1993) Carbon–carbon materials and composites. William Andrew Publishing/Noyes, New York, NY
2. Ohlhorst CW, Vaughn WL, Ransone PO, Tsou H-T (2004) Thermal conductivity database of various structural carbon–carbon composite, Materials, NASA Technical Memorandum 4787. National Aeronautics and Space Administration, Langley Research Center, Hampton, Virginia, pp 23681–24199
3. Klett JW, Ervin VJ, Edie DD (2005) Compos Sci Technol 227:56
4. Sullins AD, Daryabeigi K (2001) Effective thermal conductivity of high porosity open cell nickel foam. AIAA pp 2001–2819, 11–14 June
5. Grujicic M, Zhao CL, Biggers SB, Kennedy JM, Morgan DR (2004) Mater Sci Eng A, submitted for publication, June 2004
6. www.comsol.com, FEMLAB 3.0a, COMSOL Inc., Burlington, MA 01803, 2004
7. MATLAB, 6th ed. (2003) The language of technical computing. The MathWorks Inc., 24 Prime Park Way, Natick, MA, 01760–1500
8. Grujicic M, Chittajallu KM (2004) Appl Surf Sci 227:56
9. Blosser M (May, 2000) Advanced metallic thermal protection systems for reusable launch vehicles, Ph.D. Dissertation, University Of Virginia
10. Morgan DR (2001) Coal based carbon foam for high temperature applications. MS thesis, University of North Texas, Denton, Texas